

Design and Experimental Evaluation of a Stable Transition Controller for Geometrically Constrained Robots¹

Prabhakar R. Pagilla² and Biao Yu

School of Mechanical and Aerospace Engineering
Oklahoma State University, Stillwater, OK 74075-5016

Abstract. This paper addresses the problem of contact transition from free motion to constrained motion for geometrically constrained robots. Constraint uncertainty can cause the robot to impact the surface with a non-zero velocity. To deal with contact transition, a new stable discontinuous transition controller is proposed. Control algorithm for a complete robot task that involves both free motion and constrained motion is also developed. Extensive experiments with the proposed control strategy were conducted with different levels of constraint uncertainty. Experimental results show much improved transition performance and force regulation. Details of the experimental platform and typical experimental results are given.

1. Introduction

This work considers the contact transition control problem from free motion to constrained motion for geometrically constrained robots. Many industrial applications of robots involve interaction between the robot and the environment. Robotic surface finishing is one such application where the robot makes and breaks contact with the workpiece in the process of surface finishing. A robot typically moves freely in its workspace before making contact with the surface. Switching from free motion to constrained motion of the robot on the surface leads to stability problems if the robot makes contact with the surface with a non-zero normal velocity.

Extensive research has been done in free motion control of robots and constrained motion/force control assuming that the robot is on the surface. A large body of research in free motion control and constrained motion/force control has been reported in [1, 2]. Most of the research in constrained motion/force control has been based on the assumption that the robot is already in contact with the constraint surface. The external environment is treated as a mechanical impedance and impedance control is used in contact transition experiments in [3, 4]. Stability and control of task transition for robots for a

compliant environment is considered in [5]. Force regulation and contact transition control using positive acceleration feedback together with a switching control strategy was developed in [6]. A new contact transition control algorithm for nonlinear mechanical systems subject to a unilateral constraint was developed in [7]. A dimensionless representation of impact behavior was developed in [8]. Recent results in non-smooth impact mechanics can be found in [9].

Most of the contact transition algorithms that have been proposed assume either the environment is compliant and/or an impact model exists for the surface that can be used in the control algorithm. Further, most of the control algorithms that have been proposed have not been experimentally verified for a complete task. In this work, we design a new stable contact transition controller based on the orthogonalization principle proposed in [1]. We show that the proposed transition controller is asymptotically stable. Extensive experiments were conducted for a robot following a surface using the proposed method. Uncertainty in the location of the constraint is considered as the main cause for impact of the robot with the constraint. Experiments were conducted with different levels of constraint uncertainty. It is shown that the performance of the proposed control methodology is much improved when compared with directly switching from free motion to constrained motion/force control.

This paper is organized as follows. Section 2 develops the dynamic model for constrained robots that is used in control design. Control design for a complete task that includes free motion, transition phase, and constrained motion are given in Section 3. The main focus in this section has been on the design of the transition controller and its stability. Experimental platform and experimental results are given in Section 4. Conclusions and future research are given in Section 5.

2 Dynamic Model for Geometrically Constrained Robots

Let the kinetic and potential energy functions of the n -link robot be given by $\mathcal{K}(q, \dot{q}) = \frac{1}{2} \dot{q}^T M(q) \dot{q}$ and $\mathcal{P}(q)$, where (q, \dot{q}) are the generalized position

¹This work was supported in part by NSF Grant CMS 9700026.

²pagilla@ceat.okstate.edu

and velocity, respectively, and $M(q) \in \mathbf{R}^{n \times n}$ is the symmetric positive definite mass matrix. Let the geometric constraint on the robot be modeled by the following unilateral constraint,

$$\phi(x(q)) \leq 0, \quad (1)$$

where $x(q)$ is the Cartesian position. The geometric constraint is assumed to be smooth. Define the following orthogonal projection matrix whose image represents the normal direction of the constraint,

$$P_\phi(q) = [\nabla\phi(x(q))][\nabla\phi(x(q))]^\top / \|\nabla\phi(x(q))\|^2$$

and the kernel of $P_\phi(q)$ gives the tangential direction of the constraint, and is given by

$$Q_\phi(q) = I - P_\phi(q)$$

The dynamics of the geometrically constrained robot is

$$M(q)\ddot{q} + C(q, \dot{q})\dot{q} + g(q) = \tau + v(q)f_n \quad (2)$$

where $C(q, \dot{q})$ is the matrix composed of Coriolis and centripetal terms, $g(q)$ is the gravity vector, τ is the generalized force applied by the motors at each joint of the robot, f_n represents the magnitude of the normal contact force, and $v(q) = J^T(q)n(x)v$ maps the normal force magnitude into corresponding joint forces, where $n(x) = \nabla\phi(x)/\|\nabla\phi(x)\|$ is the unit surface normal vector in Cartesian coordinates, and $J^T(q)$ is the Jacobian of the manipulator. Further, notice that we have neglected the tangential component of the contact force. The tangential component arises mainly due to friction between the surface and robot end-effector and we assume this to be small compared to the normal force.

A complete task of the robot where the robot in the presence of the unilateral constraint can be divided into three phases: (a) when $\phi(q) < 0$, then $f_n = 0$, and the robot is said to be in free motion phase, (b) when $\phi(q) = 0$ and $f_n > 0$, then the robot is said to be in the constrained motion phase, and (c) transition from free motion phase to constrained motion phase is termed as the transition phase. The presence of the unilateral constraint in the robot workspace divides the workspace into the following sets:

$$X_c := \{q \in \mathbf{R}^n : \phi(q) = 0\} \quad (3)$$

$$X_u := \{q \in \mathbf{R}^n : \phi(q) < 0\} \quad (4)$$

$$X_f := \{q \in \mathbf{R}^n : \phi(q) > 0\} \quad (5)$$

where X_c represents the robot configurations wherein the robot lies on the constraint surface, X_u represents configurations that the robot can freely move, and X_f represents the configurations that violate the

constraint. The space X_c can be sub-divided into the sets X_{ct} and X_{ca} , i.e. $X_c = X_{ct} \cup X_{ca}$, where

$$X_{ct} := \{q, \dot{q} \in \mathbf{R}^n : \phi(q) = 0, P_\phi(q)\dot{q} \neq 0\} \quad (6)$$

$$X_{ca} := \{q, \dot{q} \in \mathbf{R}^n : \phi(q) = 0, P_\phi(q)\dot{q} = 0\} \quad (7)$$

where $P_\phi\dot{q}$ indicates the velocity normal to constraint surface. The transition of the robot between X_{ct} and X_u is precisely the transition phase. With the division of the robot workspace, the dynamics in each phase can be written as follows:

If $q \in X_u$ then the dynamic equations are

$$M(q)\ddot{q} + C(q, \dot{q})\dot{q} + g(q) = \tau. \quad (8)$$

If $q \in X_{ct}$ then the jump condition for equation (8) is given by

$$\dot{q}_+ = \mathcal{D}(q, \dot{q}_-). \quad (9)$$

If $q \in X_{ca}$, the robot end-effector is on the constraint surface and the dynamic equations are

$$M(q)\ddot{q} + C(q, \dot{q})\dot{q} + g(q) = \tau + v(q)f_n. \quad (10)$$

When the robot configuration lies in X_{ct} then the jump discontinuity for the differential equation (8) is given by (9). In equation (9), \dot{q}_+ and \dot{q}_- represent the pre-impact velocity and the post-impact velocities, respectively, and $\mathcal{D}(\cdot)$ represents an operator which maps the pre-impact velocity to post-impact velocity. This operator can take several forms depending on the choice of the impact model for the constraint surface. For example, Newton's impact model gives $\mathcal{D}(q, \dot{q}_-) = -\varepsilon \dot{q}_-$, where ε is called the coefficient of restitution.

In this paper, all we require from an impact model is that the magnitude of the rebound velocity be smaller than the magnitude of impact velocity in some metric, i.e. $\|\dot{q}_+\| = \|\mathcal{D}(q, \dot{q}_-)\| < \|\dot{q}_-\|$. For example, we require that the coefficient of restitution be smaller than 1.0 for Newton's impact model. We do not use the impact model in the control algorithm. We also assume that in the transition phase when the bounces become very small, i.e. when the impact velocity becomes very small, we characterize this by say $P_\phi\dot{q} < \delta$, then there is enough normal friction such that the system sticks to the surface. For example, Newton's impact model states that the rebound velocity decreases geometrically. Since the geometric ratio is coefficient of restitution, and is less than 1.0, which means that the bounces die down in finite time but the number of bounces are infinite. But this is seldom true for a practical case, as has been observed from contact transition control experiments in [7] for a robot interacting with a rigid surface.

When the robot lies on the constraint surface, i.e. $\phi(q) = 0$, the following relation is true: $P_\phi(q)\dot{q} = 0$. This relation means that on the constraint surface the

generalized velocity of the robot projected normal to the constraint surface must be zero for the robot to stay on the surface.

The left-hand-side of the robot dynamics (8) is linear in terms of coupled manipulator inertial parameters, and can be written as

$$M(q)\ddot{q} + C(q, \dot{q})\dot{q} + g(q) = Y(q, \dot{q}, \ddot{q})\beta$$

where β is the coupled manipulator parameter vector, and $Y(q, \dot{q}, \ddot{q})$ is a matrix.

3 Control Design

The control goal in free motion phase is to track the desired motion trajectory considering manipulator model uncertainties. During constrained motion phase, the control goal is to simultaneously track the desired motion in tangential direction, regulate the desired force normal to the constraint surface. Control of transition from free motion to constrained motion is the main focus of this section. The main goal is to design a stable transition controller. Switching directly to simultaneous motion and force control in the constrained motion could lead to severe repeated impact of the robot on the surface. A stable transition controller assures that repeated impacts do not occur. In the following control laws for each phase is proposed. Focus will be on the transition control design.

3.1 Model-based adaptive control for free motion

During this phase the robot is in free motion. An experimentally well tested model based adaptive controller considering robot parameter uncertainties is chosen. The adaptive model-based control law and parameter adaptation law are

$$\tau(t) = Y(q, \dot{q}, \ddot{q}_r)\hat{\beta}(t) - F_v e_v \quad (11)$$

$$\hat{\beta}(t) = \beta_0 - \int_0^t \Gamma^{-T} Y^T(q, \dot{q}, \ddot{q}_r) e_v dt \quad (12)$$

where F_v, Γ are the positive definite gain matrices, $\hat{\beta}$ and β_0 are the estimate and initial known value of β , respectively, $e = q - q_d$, $\dot{q}_r = \dot{q}_d - \Lambda_p e$, $\ddot{q}_r = \ddot{q}_d - \Lambda_p \dot{e} - \Lambda_i e$, $e_v = \dot{q} - \dot{q}_r$, Λ_p and Λ_i are positive definite gain matrices, and

$$Y(q, \dot{q}, \ddot{q}_r)\hat{\beta}(t) = \hat{M}(q)\ddot{q}_r + \hat{C}(q, \dot{q})\dot{q}_r$$

Substituting the control law (11) into the free robot dynamics (8) and rearranging terms results in the following error dynamics

$$M(q)\dot{e}_v + C(q, \dot{q})e_v + F_v e_v = Y(\cdot)\tilde{\beta} \quad (13)$$

where $\tilde{\beta} = \hat{\beta} - \beta$ is the parameter estimation error. Stability of the closed-loop system can be shown using Lyapunov's second method.

3.2 Impact control during transition phase

Transition phase starts when the robot makes its first impact with the surface. Then, we project the desired trajectory into tangential direction of the surface using the tangential projection matrix Q_ϕ . The desired motion trajectory of the robot is developed based on apriori knowledge of the location of the constraint. The first impact gives the actual location of the constraint surface. After the first impact, the desired trajectory, $(q_d, \dot{q}_d, \ddot{q}_d)$, is modified such that the desired velocity and acceleration in normal direction are zero, i.e. $P_\phi \dot{q}_d = 0$. Control laws are designed in tangential and normal subspace using the projection matrix and then combined. In the tangential subspace, a model-based control law similar to one given in the free motion phase is chosen.

$$\tau_t = Y(q, \dot{q}, \ddot{q}_{rt})\hat{\beta} - F_v e_{vt} \quad (14)$$

where $\dot{q}_{rt} = Q_\phi(q)\dot{q}_r$, $\ddot{q}_{rt} = Q_\phi\ddot{q}_r + \dot{Q}_\phi\dot{q}_r$, $e_{vt} = Q_\phi e_v$. In the normal subspace, the control goal is convergence of the normal velocity to zero as quickly as possible. The control law for the transition phase in normal direction is chosen as follows:

$$\tau_n = Y(q, \dot{q}, \ddot{q}_{rn})\hat{\beta} - F_v e_{vn} - \lambda_{tn} P_\phi \text{sgn}(e_{vn})$$

where $\dot{q}_{rn} = P_\phi(q)\dot{q}_r$, $\ddot{q}_{rn} = P_\phi\ddot{q}_r + \dot{P}_\phi\dot{q}_r$, $e_{vt} = P_\phi e_v$. The transition controller for both normal and tangential directions is:

$$\begin{aligned} \tau &= \tau_t + \tau_n \quad (15) \\ &= Y(q, \dot{q}, \ddot{q}_r)\hat{\beta} - F_v e_v - \lambda_{tn} P_\phi \text{sgn}(e_{vn}) \end{aligned}$$

Substituting the control law into the dynamic equations we obtain the error dynamics

$$\begin{aligned} M(q)\dot{e}_v + C(q, \dot{q})e_v + F_v e_v \\ = Y(\cdot)\tilde{\beta} - \lambda_{tn} P_\phi \text{sgn}(e_{vn}) \quad (16) \end{aligned}$$

Stability of Transition Phase: Consider the following Lyapunov function candidate,

$$V(e_v, \tilde{\beta}) = \frac{1}{2} e_v^T M(q) e_v + \frac{1}{2} \tilde{\beta}^T \Gamma \tilde{\beta} \quad (17)$$

Taking the derivative of the Lyapunov function candidate along the trajectories of (16) and simplifying we obtain

$$\dot{V}(e_v) = -e_v^T F_v e_v - \lambda_{tn} e_v^T P_\phi \text{sgn}(e_{vn}). \quad (18)$$

Since $e_{vn} = P_\phi e_v$, the derivative can be bounded by

$$\dot{V}(e_v) \leq -\sigma_v \|e_v\|^2 - \lambda_{tn} \|P_\phi e_v\|_1. \quad (19)$$

Therefore, (17) and (19) means that $V(e_v, \tilde{\beta})$ is indeed a Lyapunov function, i.e. V is positive definite and its time-derivative along the trajectories of (16) is negative definite. Using Lyapunov theorem e_v and $\tilde{\beta}$ are bounded. Further since e_v appears explicitly in \dot{V} , e_v converges to zero asymptotically.

3.3 Motion and Force Control

When the transition phase dies down, i.e. the velocity normal to the surface becomes zero, then the robot is in stable contact with the surface. At this time we switch to constrained motion control, i.e. motion control in the tangential direction and force control in the normal direction. During this phase, manipulator dynamics is

$$M(q)\ddot{q} + C(q, \dot{q})\dot{q} = \tau + v(q)f_n \quad (20)$$

It is assumed that the manipulator inertia parameters are known, the control law during this phase is chosen to be

$$\tau = M(q)\ddot{q}_r + C(q, \dot{q})\dot{q}_r - F_v e_v - \bar{v}(q)f_{nd} \quad (21)$$

where f_{nd} is the desired normal force, $e_v = \dot{q} - \dot{q}_r$, $\bar{v}(q) = v(q)/\|v(q)\|^2$, $e_{fn} = f_n - f_{nd}$, and

$$\begin{aligned} \dot{q}_r &= Q_\phi(\dot{q}_d - \Lambda_p e) + \beta_f \bar{v}(q) \int_0^t e_{fn}(\omega) d\omega \\ \ddot{q}_r &= Q_\phi(\ddot{q}_d - \Lambda_p \dot{e}) \dot{Q}_\phi(\dot{q}_d - \Lambda_p e) \\ &\quad + \beta_f \bar{v}(q) e_{fn} + \beta_f \dot{\bar{v}}(q) \int_0^t e_{fn}(\omega) d\omega \end{aligned}$$

The error dynamics under this control is

$$M(q)\dot{e}_v + C(q, \dot{q})e_v + F_v e_v = v(q)e_{fn} \quad (22)$$

Stability for this phase can be shown using an approach given in [1]. Stability of the entire control algorithm that includes the three phases can be shown along similar lines as that in [7].

4 Experiments

4.1 Experimental Platform

The experimental platform for surface following consists of a two-link robot system, a computer for real-time control, and a constraint fixture as shown in Fig. 1. The main part of the robot system is a two-axis direct drive manipulator as shown in Fig. 1. Each axis is driven by an NSK-Megatorque direct drive servo-motor which is capable of up to 3 revolutions per second maximum velocity and position feedback resolution of up to 156,400 counts per revolution. The base motor delivers up to 245 N-m of torque output, and the elbow motor delivers up to 40 N-m torque output.

The dynamics of the two-link manipulator is given by

$$M(q)\ddot{q} + C(q, \dot{q})\dot{q} = u \quad (23)$$

where the mass matrix, $M(q)$, and Coriolis matrix, $C(q, \dot{q})$, are linear in terms of unknown coupled manipulator inertial parameters. Hence the left hand

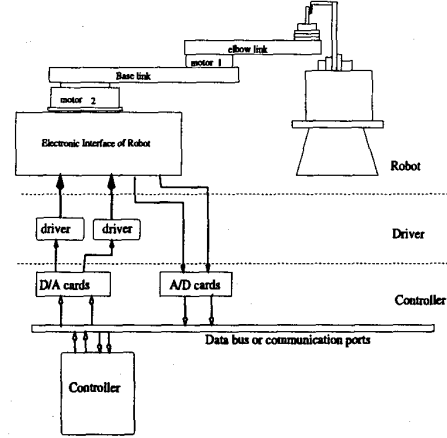


Figure 1: Schematic of Robotic Surface Following System

side of (23) can be written as

$$M(q)\ddot{q} + C(q, \dot{q})\dot{q} = Y(q, \dot{q}, \ddot{q})\beta$$

where $\beta = [p_1, p_2, p_3]^T$ is the manipulator parameter vector, and $Y(q, \dot{q}, \ddot{q})$ is the regressor matrix

$$Y = \begin{bmatrix} \ddot{q}_1 & \ddot{q}_2 & c_2(2\ddot{q}_1 + \ddot{q}_2) - s_2\dot{q}_2(2\dot{q}_1 + \dot{q}_2) \\ 0 & \ddot{q}_1 + \ddot{q}_2 & \ddot{q}_1 c_2 + \dot{q}_1^2 s_2 \end{bmatrix}$$

where $c_2 = \cos(q_2)$ and $s_2 = \sin(q_2)$.

A six-axis Force/Torque sensor is mounted on the end of the second-link of the robot manipulator. The force sensor has an on-board DSP which can provide force sensor data up to 3 KHz. Provision is also available for tool weight offset, filtering, temperature compensation, and coordinate frame rotation. The Computer system consists of a workstation, the direct drive manipulator controller and I/O cards associated with the sensors. The direct drive manipulator controller is used for real-time control and data acquisition. The controller is a three-processor system consisting of a host Pentium processor, a servo DSP and a force/torque sensor DSP.

The constraint surface $\phi(x(q))$ is chosen as a rigid straight wall, which is a thick aluminum sheet firmly held by a vice, see Fig. 1. Fig. 2 illustrates the two-link robot (top view) and the constraint surface in Cartesian space, where d is the location of the constraint on the x-axis and α is the angle between the constraint and the y-axis. The uncertainty in the constraint location is represented by ζ .

Fig. 3 shows the desired trajectory of the robot and also the constraint uncertainty that can lead to impact. In Fig. 3, the desired trajectory of the robot is CDABC (bold line). Notice that at A the robot may impact the constraint due to constraint uncertainty. Desired trajectory is designed such that without any uncertainty in the location of the constraint

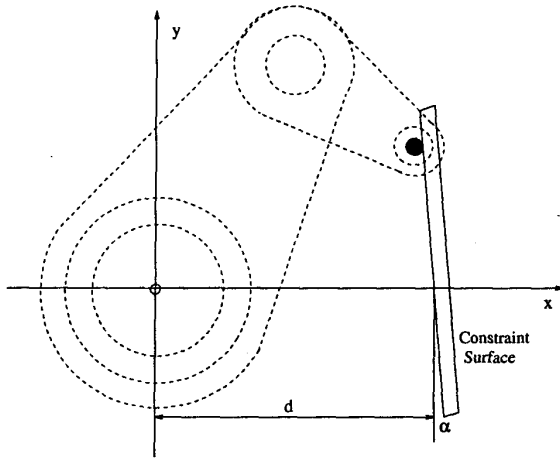


Figure 2: Robot and Constraint

the robot lands on the constraint surface smoothly, i.e. there is no normal velocity at contact.

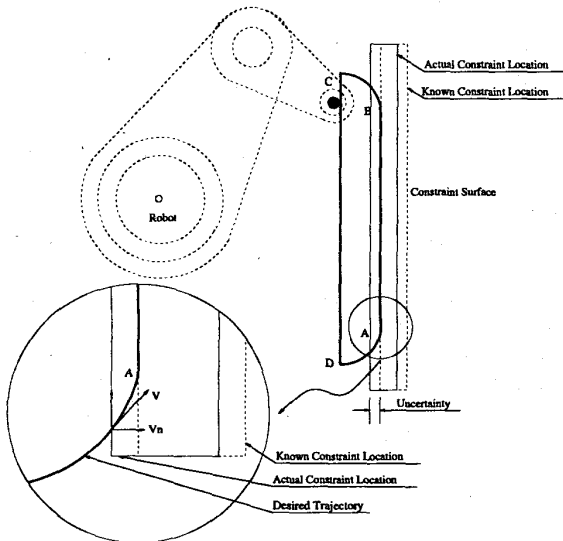


Figure 3: Desired Trajectory and Constraint Uncertainty

4.2 Experimental Results

Extensive experiments were conducted with the proposed control methodology with different levels of constraint uncertainty and different velocities of impact. We present typical experimental results in this paper. The experimental procedure is to follow the desired trajectory CDABC as shown in Fig. 3. Free motion control is applied in the trajectory sections CD, DA, and BC. Constrained motion and force control is applied along the surface AB. Transition control is activated at the first impact when switch-

ing from free motion to constrained motion. Figs. 4,

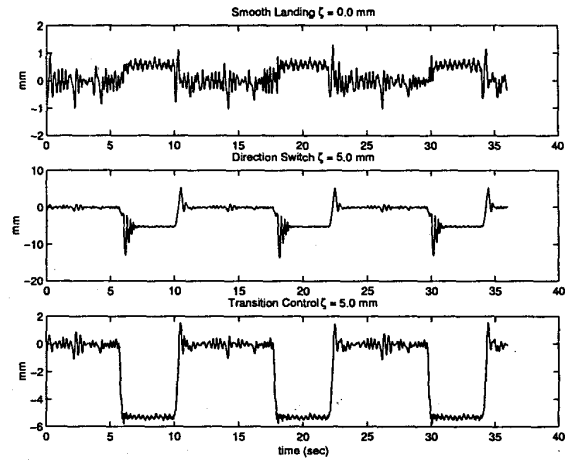


Figure 4: Normal Position

5, 6 give the normal position error, normal force, and Cartesian trajectory, respectively, for three cases: (i) smooth landing, $\zeta = 0.0 \text{ mm}$; (ii) direct switch from free motion to constrained motion control (i.e., no transition control), $\zeta = 5.0 \text{ mm}$; and (iii) with transition control at impact, $\zeta = 5.0 \text{ mm}$. Figs. 4 and 5 is for three cycles of the desired trajectory, and Fig. 6 is for one cycle. The desired normal force is 45 N. We use the same control gains used in all the experimental results shown. Notice that if we do not apply any transition control at impact the robot bounces severely on the constraint surface (see the middle graph of each figure). When we apply the transition controller the robot settles on the surface after the first bounce. For the direct switch case, it should be noticed that the end-effector tip seems to go into the surface, this is due to the compliance of the end-effector assembly.

Fig. 7 gives the L_2 norm of the normal force error for direct switch and with transition control. With no constraint uncertainty, $\zeta = 0.0 \text{ mm}$, both direct switch and transition control give similar performance. With constraint uncertainties 2.5 mm and 5.0 mm, the performance is much better if we use the transition controller. The effectiveness of the transition controller and the entire control strategy is confirmed by these experimental results.

5 Conclusion

In this paper, we proposed a control algorithm for geometrically constrained robots. Constraint uncertainty will cause impact of the robot with the surface. Control of transition from free motion to constrained motion is essential to maintain stability of the system when the constraint location is uncertain. A stable discontinuous controller is proposed

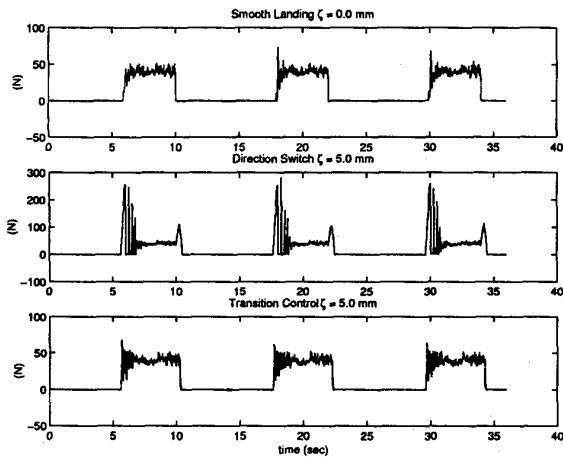


Figure 5: Normal Force

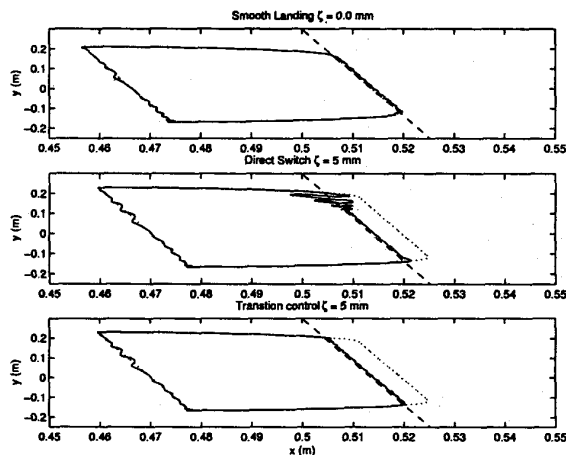


Figure 6: Cartesian Trajectory

for the transition phase. Extensive experiments were conducted with different levels of constraint uncertainty and also with different levels of impact velocity. Experimental results validate the effectiveness of the proposed control strategy. Future research will focus on actual robotic surface finishing experiments using the proposed control strategy. In future, we also plan to investigate the effects of surface compliance.

References

[1] S. Arimoto, "Control Theory of non-linear mechanical systems- a passivity-based and circuit - theoretic approach," Oxford Univ. Press Inc., New York, 1996.
 [2] D. Wang and N.H. McClamroch, "Position and Force Control for Constrained Manipulator Motion: Lyapunov's Direct Method," *IEEE Transactions on Robotics and Automation*, vol. 9, no. 3, pp. 308-312, 1993.
 [3] N. Hogan, "Impedance Control: An Approach to Manipulation: Part I - Theory; Part II - Implementation;

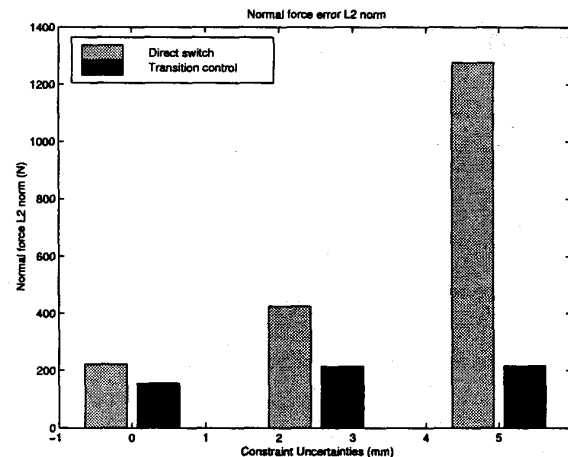


Figure 7: Normal force error L_2 norm

Part III - Applications," *ASME Journal of Dynamic Systems, Measurement and Control*, vol. 107, pp. 1-24, 1985.
 [4] H. Kazerooni, T. Sheridan and P. Houpt, "Robust Compliant Motion for Manipulators," *IEEE Transactions on Robotics and Automation*, vol. 2, no. 2, pp. 83-105, 1986.
 [5] J.K. Mills and D.M. Lokhorst, "Stability and Control of Robotic Manipulators During Contact/Non-contact Task Transition," *IEEE Transactions on Robotics and Automation*, vol. 9, no. 3, pp. 335-346, 1993.
 [6] T.J. Tarn, Y. Wu, N. Xi and A. Isidori, "Force Regulation and Contact Transition Control," *IEEE Control Systems Magazine*, February, pp. 32-40, 1996.
 [7] P.R. Pagilla and M. Tomizuka, "Contact Transition Control of Nonlinear Mechanical Systems Subject to a Unilateral Constraint," *ASME Journal of Dynamic Systems, Measurement and Control*, vol. 119, pp. 749-759, 1997.
 [8] K. Youcef-Toumi and D.A. Gutz, "Impact and Force Control: Modeling and Experiments," *ASME Journal of Dynamic Systems, Measurement and Control*, vol. 116, no. 1, pp. 89-98, 1994.
 [9] B. Brogliato, *Nonsmooth Impact Mechanics: Models, Dynamics, and Control*, Springer-Verlag, London, 1996.
 [10] L.L. Whitcomb and S. Arimoto, "Adaptive Model-Based Hybrid Control of Geometrically Constrained Robot Arms," *IEEE Transactions on Robotics and Automation*, vol. 13, no. 1, pp.105-116, 1997.
 [11] R. Volpe and P. Kholsa, "A Theoretical and Experimental Investigation of Explicit Force Control Strategies for Manipulators," *IEEE Transactions on Automatic Control*, vol. 38, no. 11, 1734-1650, 1993.
 [12] M. Raibert and J. Craig, "Hybrid Position/Force Control of Manipulators," *ASME Journal of Dynamic Systems, Measurement, and Control*, vol. 102, pp. 126-133, 1981.